Photo electron emission microscopy of polarity-patterned materials

2005 J. Phys.: Condens. Matter 17 S1415

(http://iopscience.iop.org/0953-8984/17/16/012)

INSTITUTE OF PHYSICS PUBLISHING JOURNAL OF PHYSICS: CONDENSED MATTER

J. Phys.: Condens. Matter **17** (2005) S1415–S1426 doi:10.1088/0953-8984/17/16/012

Photo electron emission microscopy of polarity-patterned materials

W-C Yang[1,2], B J Rodriguez[1], A Gruverman[1] and R J Nemanich[1]

[1] Department of Physics, and Materials Science and Engineering, North Carolina State University, Raleigh, NC 27695-8202, USA
[2] Department of Physics, Dongguk University, Seoul, 100-715, Korea

E-mail: Robert_Nemanich@ncsu.edu

Received 9 December 2004, in final form 9 December 2004
Published 8 April 2005
Online at stacks.iop.org/JPhysCM/17/S1415

Abstract

This study presents variable photon energy photo electron emission microscopy (PEEM) of polarity-patterned epitaxial GaN films, and ferroelectric $LiNbO_3$ (LNO) single crystals and $PbZrTiO_3$ (PZT) thin films. The photo electrons were excited with spontaneous emission from the tunable UV free electron laser (FEL) at Duke University. We report PEEM observation of polarity contrast and measurement of the photothreshold of each polar region of the materials. For a cleaned GaN film with laterally patterned Ga- and N-face polarities, we found a higher photoelectric yield from the N-face regions compared with the Ga-face regions. Through the photon energy dependent contrast in the PEEM images of the surfaces, we can deduce that the threshold of the N-face region is less than ∼4.9 eV while that of the Ga-face regions is greater than 6.3 eV. In both LNO and PZT, bright emission was detected from the negatively poled domains, indicating that the emission threshold of the negative domain is lower than that of the positive domain. For LNO, the measured photothreshold was ∼4.6 eV at the negative domain and ∼6.2 eV at the positive domain, while for PZT, the threshold of the negative domain was less than 4.3 eV. Moreover, PEEM observation of the PZT surface at elevated temperatures displayed that the domain contrast disappeared near the Curie temperature of ∼300 °C. The PEEM polarity contrast of the polar materials is discussed in terms of internal screening from free carriers and defects and the external screening due to adsorbed ions.

1. Introduction

Polar materials have unique surface properties associated with the spontaneous and piezoelectric polarization, which induces macroscopic polarization charges at the surface [1–3]. An electrostatic instability results from the presence of this macroscopic dipole, which can

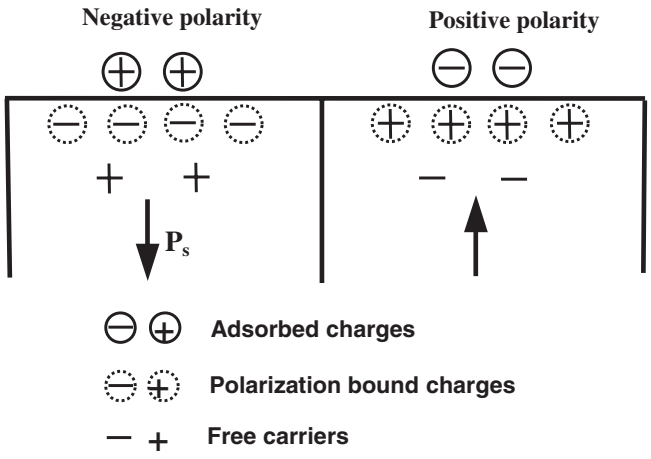

Figure 1. A schematic diagram of surface charges of polar materials. The arrow indicates the orientation of the spontaneous polarization at the surface.

be cancelled by the introduction of compensating charges. The polarization induced bound charges at the surface are screened by free charge carriers and defects in the bulk (internal screening) and/or by surface adsorption of charged molecules from the environment (external screening). The internal and external screening of the polarization can modify the surface electronic structure and the corresponding energy bands at the surface. The internal electric field near the surface created by the internal screening leads to surface band bending [1, 2] while the surface dipole induced by external screening can give rise to a variation in the surface electron affinity [3, 4]. Thus, the surface electronic properties of polar materials are controlled by the orientation of the polarization, which determines the sign of the polarization bound charge and the internal and external screening charges. Figure 1 shows a schematic diagram of the distribution of the surface charges on the positive and negative polarity surfaces. On the surface region with positive polarity, a positive polarization bound charge is compensated by absorption of negative ions from the air and/or free electrons or negatively ionized acceptors or defects in the bulk while on the negative polarity region, a negative polarization charge should be screened by adsorption of positive ions and free holes or positively ionized donors or defects.

Recently, engineering of laterally polarity-patterned structures and precise control of domain polarity in polar materials domains have become of interest. For instance, intentionally grown GaN based lateral polarity heterostructures, in which Ga- and N-face regions were grown laterally on the same surface and separated by inversion domain boundaries, can be employed for potential application in optoelectric devices [5]. Also, manipulating atomic polarization in ferroelectric substrates can be employed for a new approach to the self-assembly of complex nanostructures on surfaces [6]. Detailed information about local polarization, charge distribution, and surface potential of a surface in polar materials is necessary for controlling the local electronic structure for many potential applications.

The surface properties of polar materials with different polarities have been characterized by scanning probe microscopy (SPM) based techniques such as piezoresponse force microscopy (PFM) [7], electrostatic force microscopy (EFM) [8], and scanning Kelvin probe microscopy (SKPM) [9]. However, the complexity of the tip–surface interactions leads to difficulties in extraction of the intrinsic material properties from the SPM based measurements [9].

In this study, we employ UV photoelectron emission microscopy (UV-PEEM) for imaging of the surfaces of polar materials with patterned polarity. In UV-PEEM the image contrast

originates from local variation in the photoelectric yield, which is usually related to the photoelectric threshold. A lateral variation in the band structures associated with the lateral variation in the polarity would then be imaged through the variation in the photoelectric yield in PEEM.

First, a GaN film with laterally patterned Ga- and N-face polarities is explored. Wurtzite GaN has a polar axis parallel to the *c* direction of the crystal lattice. Deviations of the real atomic charge distributions from the point charge of the ideal wurtzite lattice give rise to its large spontaneous polarization [10], which leads to a polarization bound charge at the surface. The orientation of the spontaneous polarization and the induced bound charges are determined by the film polarity (Ga- or N-face). The Ga-face surface exhibits a negative bound charge, and the N-face surface exhibits a positive bound charge. The screening of these bound charges gives rise to surface band bending. We will establish how these effects are manifested in PEEM images of GaN films with different local polarities.

Secondly, polar surfaces of a periodically poled lithium niobate (PPLN) single crystal are explored. Unlike GaN, which is piezoelectric and pyroelectric, ferroelectrics are piezoelectric, pyroelectric, and have a spontaneous polarization that can be switched between stable polarization states (two 180° domains in lithium niobate). Below the Curie temperature (1210 °C) $LiNbO_3$ (LNO) has a hexagonal crystal structure, where the *c*-axis displacement of positive point charges (Li^+ and Nb^+) with respect to oxygen atom position leads to a ferroelectric phase. In PPLN with alternative $+c$ and $-c$ faces, the screening of the spontaneous polarization gives rise to a variation in the electron affinity and band bending in each domain. We investigate these effects on the ferroelectric domain contrast in the PEEM.

Finally, domain contrast and temperature stability of a lead zirconate titanate ($PbZrTiO_3$ (PZT)) ferroelectric film are explored. In the perovskite structure of PZT, the displacement of the O^{2-} and Ti^{4+}/Zr^{4+} ions within a unit cell gives rise to a ferroelectric phase below the Curie temperature. The transition temperature is dependent on the doping and composition of the film. Through temperature dependent PEEM images of the domain contrast, we can determine the Curie temperature of the film and a variation of the spontaneous polarization via the pyroelectric effects.

In particular, with tunable UV free electron laser (FEL) excitation, we determine the photothreshold and the variation in the electron affinity of different polar regions. The PEEM polarity contrast of the polar materials is discussed in terms of the surface band bending and the electron affinity variation induced by the polarization bound charges and surface adsorbates.

2. Experimental systems

The experiments were performed in a UV-PEEM (Elmitec PEEM-III) system combined with the ultra-violet free electron laser (UV-FEL) located at the Duke University Free Electron Laser Laboratory. Figure 2 shows a schematic diagram of a UV-FEL PEEM system. The system is connected via a UHV sample transfer system to a custom gas source molecular beam epitaxy (GSMBE) system, which allows *in situ* studies of the film growth and surface treatments. The base pressure of the PEEM system was $<2 \times 10^{-10}$ Torr. This system has a predicted and demonstrated resolution of ∼10 nm at a 10 000× magnification [11]. The electric potential used for accelerating the imaging electrons is approximately 20 kV across a gap of ∼2 mm.

The incident UV light is obtained from the tunable spontaneous emission of the UV-FEL with photon energies from 4.0 to 6.3 eV with an energy full width at half-maximum of ∼0.1 eV [11]. The spontaneous radiation of the FEL is pulsed with a repetition rate of 30 MHz (ten bunches) and a pulse duration of ∼100 ps. The output power depends on the energy and current of the electron beam in the synchrotron [12]. In these experiments, the synchrotron was

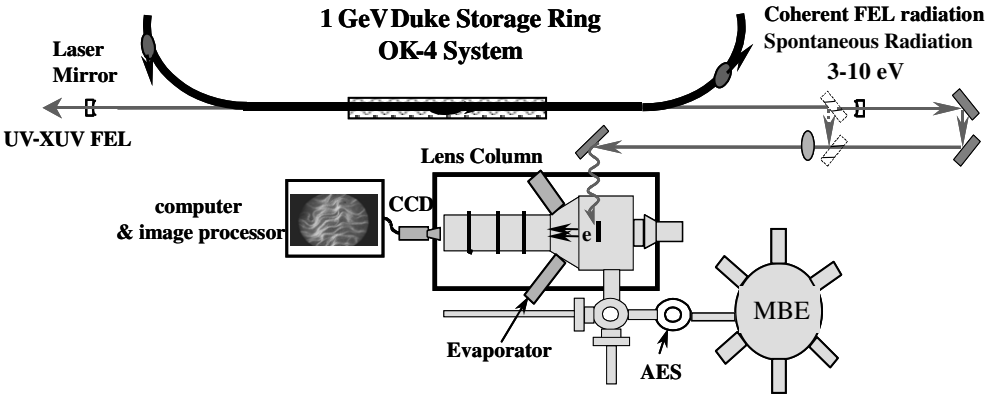

Figure 2. A schematic diagram of the UV-FEL (not to scale) and PEEM system. The UV light is supplied in spontaneous emission mode using mirrors shown dotted or in the lasing mode using the mirrors shown with darker lines.

operated at an electron energy of 0.28 GeV and current of >150 mA. This operation provided us with UV spontaneous radiation with an average power of ∼2 mW and a corresponding peak power of ∼20 W. To deliver and focus the beam to the sample in the PEEM, three UV mirrors and a 1 m focal length fused silica lens are installed between the light output window and the PEEM. The incident angle of the beam is 15° with respect to the sample surface. The focused beam was elliptical in shape with a size of ∼20 μm × 100 μm. This corresponds to an average power density of ∼1 W cm^{-2}. The capabilities of the FEL-PEEM are described in more detail elsewhere [11].

PEEM images are enhanced with a microchannel plate and displayed on a phosphor screen. The images were observed with a CCD camera, and stored digitally with an image processor. For the data presented here, sixteen successive frames were integrated to form an image. The resulting images correspond to an integrated signal of 16/30th of a second.

3. Results and discussion

3.1. GaN film with laterally patterned Ga- and N-face polarity

Polarity contrast and local intensity enhancement of a GaN film with laterally different polarities are investigated [13]. A GaN film with laterally patterned Ga- and N-face polarities was fabricated using plasma induced molecular beam epitaxy (PIMBE). The Ga-face GaN (1 μm thick) was grown on an AlN nucleation layer (10 nm thick), while the N-face GaN (1 μm thick) was grown directly on the sapphire substrate [14]. The inversion domain boundaries (IDBs) are created at the boundaries between the Ga- and N-face GaN. The free electron concentration of the film was determined as $\sim N_d = 3.3 \times 10^{17}$ cm^{-3} (n-type) by Raman scattering measurements. To remove oxygen and carbon contaminants, the film was cleaned *in situ* by an ammonia based, high temperature chemical vapour clean (CVC) [15] in the UHV GSMBE chamber, which is connected to the PEEM chamber.

Figure 3 displays PEEM images of an IDB region of the GaN film before and after *in situ* cleaning. For the as-loaded GaN surface, the brightness contrast between the Ga- and N-face regions is not apparent (figure 3(a)). For photon energies from 5.0 to 6.3 eV, the contrast did not change, but the whole surface became slightly brighter at higher photon energies. However, after the cleaning process, the contrast between the different polarity regions was

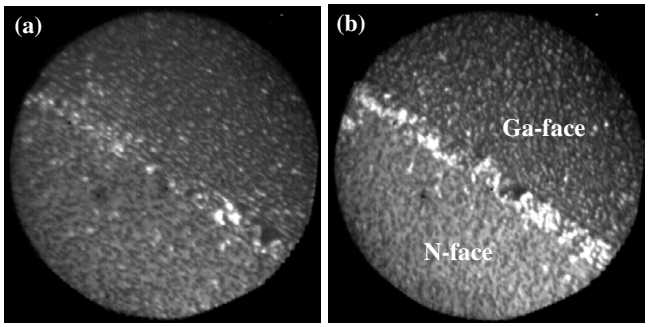

Figure 3. PEEM images of an IDB region of GaN based lateral polarity heterostructure (a) before the CVC process and (b) after the CVC process. The field of view is 20 μm, and the FEL photon energy is 5.6 eV.

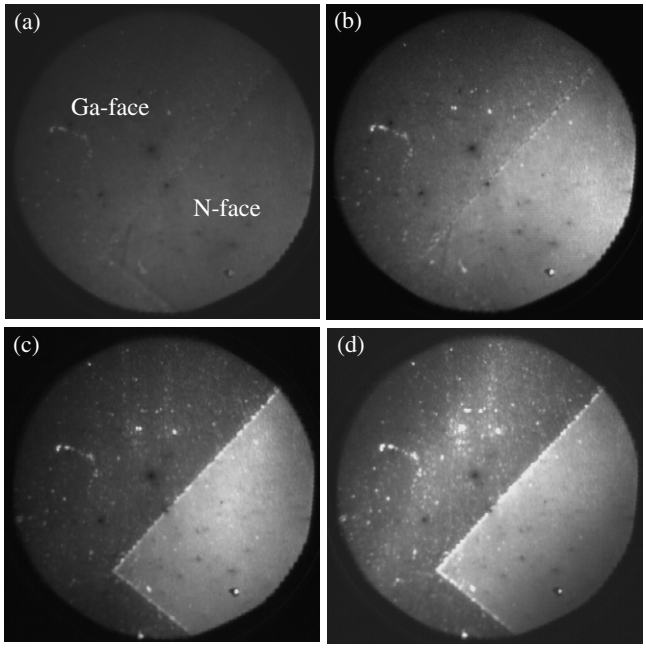

Figure 4. PEEM images of the CVC-cleaned GaN film showing the lateral polarity heterostructure. The images were obtained with photon energies of (a) 4.8 eV, (b) 4.9 eV, (c) 5.6 eV, and (d) 6.3 eV, respectively. The field of view is 150 μm.

significantly enhanced (figure 3(b)). Through comparison of high magnification PEEM and AFM topography images [13], we could identify the polarity of the specific surface regions. The darker region in the PEEM is recognized as a Ga-face surface while the brighter region is a N-face surface. In addition, relatively strong emission intensity was detected from the inversion domain boundary regions (IDBRs).

To explore the electronic properties of the different regions, we obtained PEEM images with photon energies from 4.5 to 6.3 eV in steps of 0.1 eV (figure 4). For photon energies below 4.8 eV, contrast between the two regions was not detected (figure 4(a)). However, for photon energies greater than 4.9 eV, emission from the N-face regions was observed, which led to a distinct emission contrast between the two domains (figure 4(b)). As the photon energy was increased from 4.8 eV, the emission from the N-face regions also increased, leading to enhanced contrast (figure 4(c)). However, at 6.3 eV the emission from the Ga-face region became more significant, and the emission contrast was relatively reduced (figure 4(d)). From the results, we can deduce that the photothreshold of the N-face region is less than $\sim$4.9 eV while that of the Ga-face regions is greater than 6.3 eV. Also, the bright emission from the IDBR indicates an emission threshold of less than 4.9 eV (figure 4(b)).

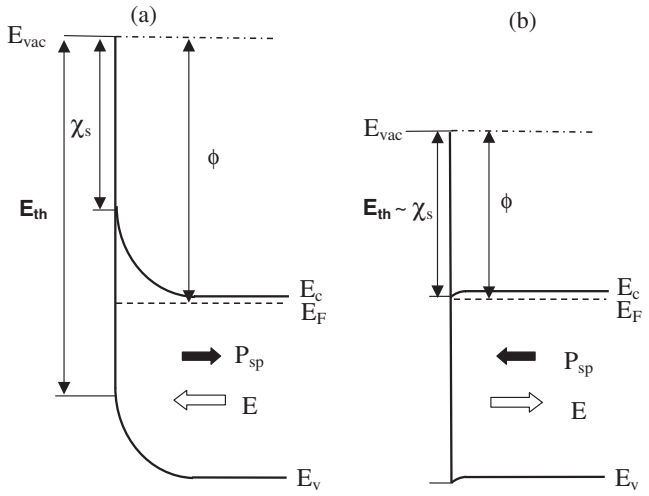

Figure 5. Energy band diagrams for (a) Ga-face and (b) N-face GaN. The quantities χ_s, ϕ, and E_{th} are the surface electron affinity, work function, and photothreshold, respectively. The arrows represent the directions of spontaneous polarization, P_{sp}, and the internal electric field, E.

To explain the much lower photothreshold at the N-face surface for the cleaned film, we considered the effect of the polarity on the band structure at each surface. In n-type GaN, the energy band diagrams for the Ga- and N-face surfaces are illustrated in figure 5. The bulk Fermi level position of our GaN film was estimated to be ∼0.05 eV below the conduction band edge for both Ga- and N-face regions [13]. For the Ga-face region, the spontaneous polarization (-0.034 C m^{-2}) points from the surface to the substrate, inducing a negative bound charge at the GaN surface ($\sigma/e = -2.12 \times 10^{13}$ cm^{-2}) (we only consider the spontaneous polarization, which dominates the total polarization [7]). The negative bound charge at the surface is screened by the positively ionized donors close to the surface. This leads to upward band bending in the depletion region at the Ga-face surface (figure 5(a)). In contrast, downward band bending should occur at the N-face surface due to the opposite direction of the spontaneous polarization. The positive bound surface charge gives rise to a free electron accumulation layer at the N-face surface, fixing the Fermi level close to the conduction band edge. This accumulation layer leads to a slight downward bending of the conduction band edge at the N-face surface (figure 5(b)).

We suggest that the surface band bending gives rise to a variation in the photothreshold at different polar surfaces. For upward band bending of the Ga-face region, the photothreshold at the bulk increases by the amount of band bending while the photothreshold at the surface does not change and is $\chi_s + E_g$ (figure 5(a)). Thus, the electrons are photoemitted from the valence band edge at the surface for a photon energy greater than $\chi_s + E_g$. On the other hand, for downward band bending of the N-face region, an electron accumulation layer results in the conduction band minimum slightly below the Fermi level. As a result, the electrons in the accumulation layer can be photoemitted from the conduction band, and the photothreshold at the surface would be essentially the electron affinity (figure 5(b)). Thus, the relatively bright intensity in the N-face regions is attributed to electron emission from the conduction band due to downward band bending. Therefore, the polarity dependent photothreshold causes a photoelectric yield difference between the Ga- and N-face regions and leads to the polarity contrast in the PEEM images of the GaN film.

Next, we discuss possible emission mechanisms for the strong intensity at the IDBRs in the PEEM images. Apparently, the intense emission was only observed from the N-face side of the IDBR [13]. The band bending difference between the Ga- and N-face surfaces can play

a significant role, which can lead to an additional emission process at the IDBRs aside from the normal electron excitation from the valence band edge. If we consider a lateral band diagram of an LPH surface in the vicinity of the IDB, the band edges will shift from the Ga face to the N face across the IDB. The induced potential energy difference, ΔE, of $\sim$1 eV results in a built-in lateral field and a surface space charge region [13]. Also, the local NaCl-like geometry of the IDB will lead to a band edge discontinuity at the IDB and a slight downward band bending from the N-face side of the IDBR. On the basis of the lateral band diagram, we can postulate two mechanisms to account for the electron emission from the IDBRs. First, for a photon energy greater than $(E_{\mathrm{th}} - \Delta E)$ and less than E_{th}, photoexcited electrons from the valence band maximum of the Ge-face side in the IDBR will be transverse to the IDB and diffuse into the N-face side in the IDBR. The diffused hot electrons at the N-face side can be emitted directly into the vacuum since they are above the vacuum level. Second, the electrons originating from the conduction band edge of the N-face side of the IDBR can directly contribute to the photoemission yield because of the downward band bending. Both effects could contribute to the intense emission from the N-face side of the IDBR.

3.2. Periodically poled ferroelectric crystals: $LiNbO_3$ (LNO)

The domain contrast and photothreshold of polar surfaces of a ferroelectric $LiNbO_3$ crystal with periodically poled domains were examined. The periodic domain structure was fabricated by lithography and electric field poling on the original $+c$ face of congruent (0001) LNO. The $+c$ face surface was photolithographically patterned and subsequently developed to produce $\sim$4.5 μm wide stripes with a periodicity of $\sim$6.8 μm. The patterned regions of the sample were engineered to produce antiparallel domains ($-c$ face regions), by applying an external electric field exceeding the intrinsic coercive field of 20 kV mm^{-1} for the crystal [22]. This technique (referred to as electric poling) is a standard method for achieving domain inversion in ferroelectrics [22].

Figure 6 displays PEEM images of the uncleaned surfaces of the as-received sample obtained with various photon energies. For photon energies below 4.5 eV, domain contrast was not detected (figure 6(a)). However, for photon energies greater than 4.6 eV, the brightness contrast between antiparallel domains is apparent (figure 6(b)). The wider domains ($\sim$4.5 μm) are brighter than the narrower domains ($\sim$2.3 μm). Through comparison of the AFM, PFM, and PEEM images, we were able to identify the polarity of the domains. The bright regions in the PEEM image are recognized as negative domains while the darker regions are positive domains; indicating relatively intense electron emission from the surface of the negative domains. As the photon energy was increased from 4.6 eV, the emission from the negative domains increased, leading to enhanced contrast (figure 6(c)). However, at 6.2 eV the emission from the positive domain became more significant, and the emission contrast was relatively reduced (figure 6(d)). From the results, we deduce that the electron photothreshold of the negative domains is $\sim$4.6 eV while that of the positive domains is greater than 6.2 eV.

To understand the origin of the PEEM polarity contrast mechanism of the ferroelectric domains, we consider the effect of the ferroelectric polarity on the band structure at the surface for each domain such as band bending and electron affinity. It is noted that due to its band gap of 3.9 eV, LNO would be considered as a wide band gap ferroelectric semiconductor. If the polarization bound charge is internally screened by a space charge layer, band bending is generated in the space charge region near the surfaces. Unfortunately, we have no direct measurement of the band bending in the near surface region of these LNO samples. Since our LNO sample is undoped, it may be reasonable to assume that any band bending that exists will occur over a length scale that will be large compared to the length scale for UV

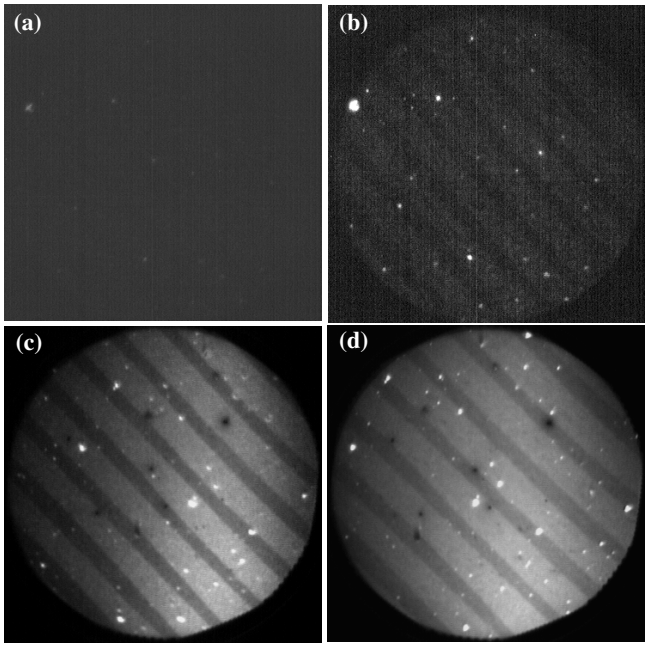

Figure 6. PEEM images of PPLN obtained with photon energies of (a) 4.5 eV, (b) 4.6 eV, (c) 5.2 eV, and (d) 6.2 eV, respectively. The field of view is 50 μm.

absorption and/or electron emission. Thus, contrary to the polarity contrast of the GaN film, the band bending effects on the emission from the undoped LNO is negligible in the PEEM measurements.

We suggest that the domain contrast of ferroelectric surfaces is predominantly due to the variation in electron affinity at each domain surface induced by the external screening. For a ferroelectric semiconductor, the screening of the polarization charges by adsorption of unidentified charged molecules or ions on a surface from the environment (external screening) will give rise to an additional surface dipole and result in a variation in the electron affinity. This effect is modelled schematically in figure 7 for the two polar LNO surfaces. The change of the electron affinity can be estimated using the following relation:

$$\Delta\chi = \frac{e^2 N\delta}{\varepsilon} = \frac{epN}{\varepsilon}$$

where N is the number of ions per unit surface area, ε is the dielectric constant of the dipole layer, and δ is the effective distance between the charge centres (dipole $p = e\delta$). The adsorbed species will be determined by the surface polarity of the ferroelectric. For a negative domain, positive ions would be adsorbed, and the electron affinity should decrease ($\Delta\chi < 0$) while for a positive domain, negative ions would be adsorbed, and the affinity should increase ($\Delta\chi > 0$). As shown in figure 7, the electron affinity variation would lead to a variation in the photothreshold at the different polar domains. For the negative domain, the photothreshold decreases by $\Delta\chi^-$ (where $E_{\rm th}^- = E_{\rm g} + \chi_{\rm s} - \Delta\chi^-$) while for the positive domain the photothreshold increases by $\Delta\chi^+$ (where $E_{\rm th}^+ = E_{\rm g} + \chi_{\rm s} + \Delta\chi^+$). Consequently, the relatively bright emission from the negative domains of the LNO is attributed to a reduction of the photothreshold due to surface adsorption of positive ions, and the PEEM polarity contrast of the LNO is attributed to the variation in the electron affinity induced by the surface adsorption of both the positive and negative domains.

The PEEM measurements shown in figure 6 indicate that the threshold difference between positive and negative domains of the air exposed surface is greater than $\sim$1.6 eV, which would

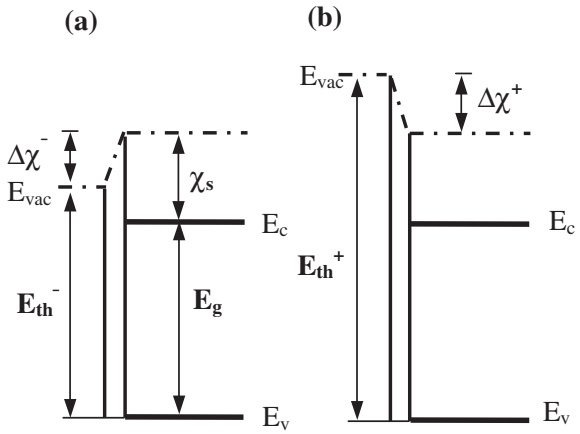

Figure 7. Energy band diagrams of adsorbate-covered $LiNbO_3$ surfaces for (a) negative and (b) positive polarity domains. The quantities χ_s, E_g, E_{th}, and $\Delta\chi$ are the surface electron affinity, band gap, photothreshold, and electron affinity variation due to surface adsorption, respectively. Superscripts represent the quantities for the negative (−) and positive (+) polarity domain. We have assumed negligible band bending in the near surface region probed by photoemission.

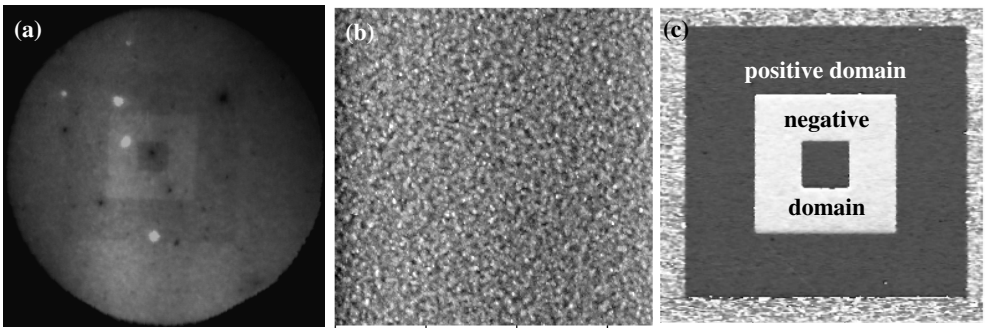

Figure 8. (a) PEEM, (b) AFM, and (c) PFM images of a polarity-patterned PZT thin film. The fields of view are (a) 50 μm and ((b) and (c)) 35 μm. All images were obtained from the same surface. The PEEM image was obtained with a photon energy of 4.8 eV. In (c), the PFM image obtained from the same region of the AFM image shows that the innermost 5×5 μm^2 square is the positive domain which is darker than the negative domain.

correspond to $\Delta\chi^- + \Delta\chi^+$. If we assume that the polarization charges are completely screened by the surface adsorption, we can estimate $N \sim P_s/q$ from the spontaneous polarization, P_s. For LNO, $N \sim 4.4 \times 10^{14}$ cm^{-2} ($P_s = 70 \times 10^{-6}$ C cm^{-2} [16]). If we assume a surface dipole layer with a charge separation distance, δ, of 0.3 nm and a dielectric constant, ε, of 31 (LNO), the $\Delta\chi$ at each domain surface will be ∼0.8 eV. This value is an estimate because the dielectric constant of the dipole layer is an ill-defined property since the dipole layer is not a bulk entity. However, this estimated value is consistent with our PEEM measurements. In addition, assuming a $\Delta\chi$ of ∼0.8 eV for each domain, we can deduce that the value of χ_s is ∼1.5 eV ($\chi_s = E_{th}^+ - E_g - \Delta\chi^+$). Photoemission studies of cleaned LNO surfaces with no adsorbates have yielded a value of the electron affinity of ∼1.1 eV [17], which is close to our results.

3.3. Polarity-patterned ferroelectric thin film: $PbZrTiO_3$ (PZT)

The domain contrast and thermal stability of a PZT thin film with patterned polarity were investigated. A 200 nm thick film of tetragonal (111)-oriented PZT was sputtered onto a Pt bottom electrode [18]. Concentric square domains of alternating opposite polarities were

patterned into the PZT by electric field poling via a conductive AFM tip. A $30 \times 30\ \mu m^2$ square was poled into a positive polarization state by application of negative voltage. Then, a $15 \times 15\ \mu m^2$ square was poled into a negative polarization state by a positive applied voltage. Finally, a $5 \times 5\ \mu m^2$ was poled into a positive polarization state by a negative applied voltage.

Figure 8(a) displays a PEEM image of the surface of the patterned regions in the as-received PZT film. The brightness contrast between antiparallel domains is apparent. The innermost square (positively poled domain) is darker than the next square (negatively poled domain), indicating relatively intense electron emission from the surface of the negative domains. The topographic AFM image (figure 8(b)) shows similar morphologies for the two domains, which suggests that the PEEM domain contrast is independent of surface topography. With PFM, a modulation voltage is applied to a conductive tip, which excites the piezoelectric sample causing it to expand and contract at the frequency of the applied signal. This technique can be used to determine polarity by monitoring the phase of the piezoresponse relative to the modulation voltage. PFM analysis of the domain pattern (figure 8(c)) confirmed that the innermost square corresponds to a positive domain. The PEEM polarity contrast of the PZT film is also explained in terms of the variation in the electron affinity induced by the surface adsorption, as suggested in our interpretation of PEEM contrast of PPLN.

To measure the photothreshold of each polar domain, PEEM images were obtained with photon energies from 4.0 to 6.3 eV. For photon energies below 4.3 eV, domain contrast was not detected, and for photon energies of 6.3 eV the contrast is significantly reduced. From the results, we deduced that the threshold of the negative domains was less than 4.3 eV while that of the positive domains was greater than 6.3 eV. To our knowledge there is no photoelectric yield difference between the different polarity surfaces of PZT films. However, for nonpolar PZT films, Schottky barrier measurements and photoemission studies have indicated an electron affinity of 1.8–3.5 eV [19, 20]. Then with a band gap of 3.4 eV, the photothreshold is expected to be ∼5.2–6.9 eV. From the PEEM measurements of the PZT films, the photothreshold difference between positive and negative domains is greater than ∼2.0 eV, which indicates that the change of the electron affinity at each domain due to surface dipole effects induced by surface adsorbates is ∼1.0 eV. Thus, if we assume that the electron affinities are equal at the two domains, we can deduce that the affinity of a nonpolar PZT surface is ∼1.9 eV and the corresponding photothreshold is ∼5.3 eV, which is consistent with this analysis.

To investigate the temperature stability of the patterned domains, we obtained PEEM images at a fixed photon energy of 5.0 eV while increasing the sample temperature to over 300 °C, as shown in figure 9. As the temperature was increased from room temperature to 250 °C, the domain contrast was reduced due to a relative reduction of the emission intensity from the negative domains (figures 9(a) and (b)). Consequently, at $\gtrsim$300 °C the contrast of the patterned domains completely disappeared (figure 9(c)). The patterned domains did not reform during cooling to room temperature (figure 9(d)). From the results, we deduce that the Curie temperature (T_c) of the PZT film is ∼300 °C, at which a phase transformation would occur from a tetragonal ferroelectric to a cubic paraelectric structure.

The reduction of the PEEM domain contrast of the film with increasing temperature can be explained in terms of a reduction in electron affinity difference between opposite domains. As the temperature of the PZT sample increases, the spontaneous polarization within the patterned region will be reduced at a rate determined by the pyroelectric coefficient (4.2×10^{-4} C K^{-1} m^{-2}). The reduction in the magnitude of the spontaneous polarization leads to a decrease in the density of the polarization bound charges and a relaxation (thermal desorption) of adsorbed screening charges at the surface, and a corresponding reduction of the surface dipole (formed between the polarization charge and the screening charge). As a result, there is a reduction in the electron affinity at each domain which leads to a reduction

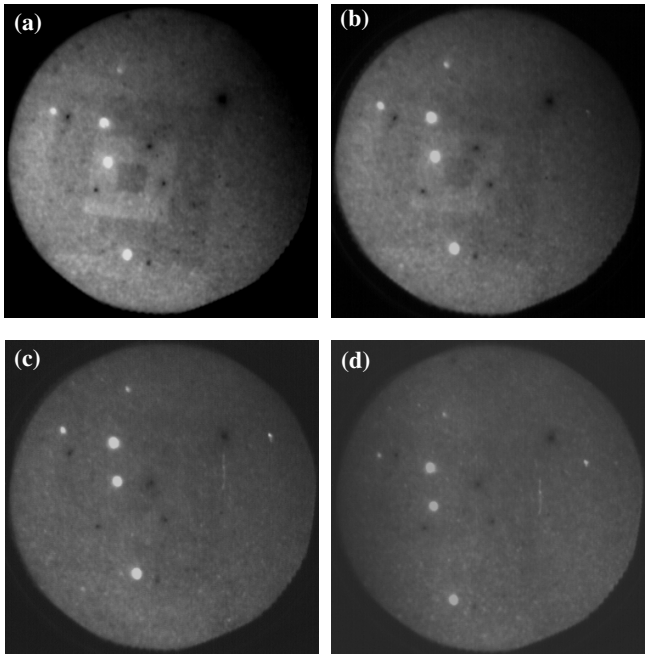

Figure 9. PEEM images of the PZT during annealing at temperatures of (a) 150 °C, (b) 250 °C, and (c) 300 °C. (d) This image was obtained after cooling to room temperature. All images were obtained with photon energy of 5.0 eV. The field of view is 50 μm.

in emission intensity and domain contrast between domains. Once the temperature reaches T_c, the PZT film is no longer ferroelectric and the PEEM polarity contrast of the domains disappears due to the equivalence of the electron affinity between domains.

As the sample is allowed to cool to room temperature, the sample will undergo a phase transition from the paraelectric to the ferroelectric phase, at which time the magnitude of the spontaneous polarization will begin to increase. Without any external electrode, the spontaneous polarization induces polarization bound charges at the surface and will create a depolarization field. To reduce the electrostatic energy due to the depolarization field, the PZT film would break up into domains of different polarizations with a certain range of domain width and form a multi-domain structure with random polarizations [21]. Thus, the domain patterns of the PZT film did not reform upon cooling the sample, which can explain why the PEEM polarity contrast could not be detected upon cooling below T_c.

4. Summary

We have used UV-PEEM to image the surfaces of polarity-patterned materials. Polarity contrast was observed between the opposite polar regions. Through the photon energy dependent contrast in the PEEM images of the surfaces, we deduced the photothreshold of each region. For a GaN based laterally polarity heterostructure, polarity contrast was observed between the Ga- and N-face regions with a higher photoyield from N-face regions, and the measured photothresholds are 4.9 eV for N-face regions and >6.3 eV for Ga-face regions of the GaN film. For a periodically poled $LiNbO_3$ and a polarity-patterned PZT, polarity contrast was observed between the positive and negative domains with more intense emission from the negative domains. The measured photothresholds of the negative domains are 4.6 eV for the LNO crystal and 4.3 eV for the PZT film while the threshold of the positive domains is greater than 6.2 eV for both ferroelectrics. In particular, the image contrast of the PZT surface disappeared

near the Curie temperature of 300 °C, which is attributed to the polarization disappearance in the patterned domains due to the structure change above the Curie temperature.

We propose that the PEEM polarity contrast of polar materials is attributable to a variation in the photoelectric yield induced by a modification of the surface band structure associated with surface polarity. The polarity contrast of the GaN film is proposed to be due to the enhanced emission from the N-face regions, which was attributed to photoemission of electrons in the conduction band at the surface induced by band bending (i.e. internal screening). In contrast, the domain contrast of the ferroelectrics is attributed to a variation in surface electron affinity associated with surface dipole layers formed by surface adsorbates (i.e. external screening).

Acknowledgments

We gratefully acknowledge the Duke Free Electron Laser Laboratory for access to the OK-4 free electron laser. This work was supported by grants through the MFEL programme administered through the AFOSR, the Office of Naval Research MURI on Polarization Electronics Contract No N00014-99-1-0729, and the NSF under Grant No DMR 0235632.

References

[1] Fridkin V M 1980 *Ferroelectric Semiconductors* (New York: Consultants Bureau)
[2] Ambacher O, Smart J, Shealy J R, Weimann N G, Chu K, Murphy M, Dimitrov R, Wittmer L, Wittmer M, Tutzmann M S, Rieger W and Hilsenbeck J 1999 *J. Appl. Phys.* **85** 3222
[3] Luth H 1993 *Surfaces and Interfaces of Solids* 2nd edn (Berlin: Springer)
[4] Yang W-C, Rodriguez B J, Gruvernman A and Nemanich R J 2004 *Appl. Phys. Lett.* **85** 2316
[5] Stutzmann M, Ambacher O, Eickhoff M, Karrer U, Lima Pimenta A, Neuberger R, Schalwig J, Dimitrov R, Schuck P and Grober R 2001 *Phys. Status Solidi* b **288** 505
[6] Kalinin S V, Bonnell D A, Alvarez T, Lei X, Hu Z and Ferris J H 2002 *Nano Lett.* **2** 589
[7] Rodriguez B J, Gruverman A, Kingon A I, Nemanich R J and Ambacher O 2002 *Appl. Phys. Lett.* **80** 4166
[8] Jones K M, Visconti P, Yun F, Baski A A and Morkoç H 2001 *Appl. Phys. Lett.* **78** 2497
[9] Kalinin S V and Bonnell D A 2001 *Phys. Rev.* B **63** 125411
[10] Stutzmann M, Ambacher O, Eickhoff M, Karrer U, Lima Pimenta A, Neuberger R, Schalwig J, Dimitrov R, Schuck P and Grober R 2001 *Phys. Status Solidi* b **288** 505
[11] Ade H, Yang W, English S, Hartman J, Davis R F, Nemanich R J, Litvinenko V N, Pinayev I V, Wu Y and Mady J M 1998 *Surf. Rev. Lett.* **5** 1257
[12] Litvinenko V N, Park S H, Pinayev I V and Wu Y 2001 *Nucl. Instrum. Methods* A **475** 240
[13] Yang W-C, Rodriguez B J, Park M, Nemanich R J, Ambacher O and Cimalla V 2003 *J. Appl. Phys.* **94** 5720
[14] Dimitrov R, Tilak V, Murphy M, Schaff W J, Eastman L F, Lima A P, Miskys C, Ambacher O and Stutzmann M 2000 *Mater. Sci. Soc. Symp.* **622** T4.6.1
[15] King S W, Barnak J P, Bremser M D, Tracy K M, Ronning C, Davis R F and Nemanich R J 1998 *J. Appl. Phys.* **84** 5248
[16] Rosenman G I, Boikova E I and Chepelev Y L 1982 *Phys. Status Solidi* a **69** k173
[17] Akhayan A A and Brozdnichenko A N 1983 *Sov. Phys.—Solid State* **25** 1990
[18] Rodriguez B J, Gruverman A, Kingon A I, Nemanich R J and Cross J S 2004 *J. Appl. Phys.* **95** 1958
[19] Shih W Y, Shih W-H and Aksay I A 1994 *Phys. Rev.* B **50** 15575
[20] Scott J F 1999 *Japan. J. Appl. Phys.* **38** 2272
[21] Zheng L, Lin C and Ma T 1996 *J. Phys. D: Appl. Phys.* **29** 457
[22] Yamada M, Nada N, Saitoh M and Watanabe K 1993 *Appl. Phys. Lett.* **62** 435